NUMERICAL OPTIMIZATION OF THE TONAL NOISE OF A BACKWARD CENTRIFUGAL FAN USING A FLOW OBSTRUCTION PART II: FLOW OBSTRUCTION OPTIMIZATION

Romain PAIN[1], Vincent LE GOFF[2], Franck PEROT[2],
Andrea SHESTOPALOV[2], Amanda LEARNED BOUCHER[2],
Min-Suk KIM[3], Xavier CARNIEL[4], Yvon GOTH[4]

[1] *EuroXA, 76 route de la demi-lune, 92057 Paris La Défense, France*

[2] *Exa Corporation, 55 Network Drive, Burlington MA, 01803, USA*

[3] *Exa Corporation, 150 North Hill Drive, Brisbane CA, 94005, USA*

[4] *CETIM, 52, avenue Félix-Louat - BP 80064. 60300 Senlis, France*

SUMMARY

This paper presents an efficient and automated digital process able to design optimized passive noise control devices known as flow obstructions. These flow obstructions are placed upstream fans in installed conditions and have been shown to be able to reduce the fan Blade Passing Frequency (BPF) noise levels by up to 13 dB. With a traditional experimental method, the design of the shape of the obstruction and its positioning requires a tries-and errors approach involving both prototypes arbitrarily chosen and time consuming and expensive experimental campaigns. Such an experimental process on one hand does not guarantee to find the best possible design and on the other hand takes time to carry out and analyze. Leveraging an association between accurate and fast aeroacoustics simulations and an advanced optimization process, an innovative numerical approach has been developed. This method is used in the present study on a production fan-heat exchanger system in order to evaluate the ability at automatically designing and positioning the most efficient flow obstructions.

INTRODUCTION

Rotating blades and especially fans are frequently sources of noise annoyance in the industry. Driven by constantly more stringent acoustic regulations, reducing the global radiated noise has therefore become one of the industry major targets. In this study a cooling module constituted of a centrifugal fan and an upstream heat exchanger is investigated. This cooling module is productively used to manage the thermal performances of heavy-duty machine engines. For this configuration the tonal contribution appears to be a significant issue and has to be reduced in order to satisfy noise

targets. The main origin of the tonal noise is related to the ingestion by the fan of a turbulent and non-uniform flow passing through the heat exchanger [1].

A study by Pérot *et al.* [1] investigates both experimentally and numerically the effect of a manually optimized passive noise control device known as a flow obstruction that is able to significantly reduce the fan BPF noise levels [2-4]. Additional appealing aspects of this passive device are on one hand to not introduce any significant penalties on the broadband levels or on the airflow performances and on the other hand to be relatively easy to install. In this study, the obstruction is located upstream the heat exchanger and centered on the fan axis. Measurements show that the BPF noise level can be reduced by 10-13 dB. To come up with these results, upfront and arbitrary choices on the design of the obstruction had to be made and involved a manual determination of the axial and angular positions of the flow obstruction. The numerical approach used in [1] and based on transient aeroacoustics predictions accurately captures the effect of the flow obstruction both on the noise and airflow performances while satisfying development turnaround times. Furthermore, the simulation results are used to provide some insight of the noise generation mechanisms highlighting the role on the BPF noise of inlet and coherent flow structures developing on the shroud and sliced by the blade.

Although the manual design optimization and calibration of the obstruction shows outstanding acoustic and airflow performances [1], the design process has to be repeated for every new system developed by manufacturers. Practically, for each new configuration, a set of possible obstructions with different shapes and sizes have to be prototyped and their optimal axial and angular positions have to be determined. This approach hence requires a lot of prototyping and tedious and extensive experimental testing that can represent a constraint during the development.

This paper aims at proposing and validating a novel numerical approach overcoming the constraints mentioned previously. The approach consists in an efficient and automated digital process able to generate and calibrate optimized flow obstruction designs in a time frame satisfying the product development cycles. In the present study, the designs of the numerically evaluated obstructions are generated using morphing features implemented in the geometry tool PowerDELTA. The Computational Fluid Dynamics/Computational AeroAcoustics (CFD/CAA) 3-D solver PowerFLOW based on the Lattice Boltzmann Method (LBM) is used to predict the turbulent flow and the associated noise [5, 7]. This CFD/CAA solver is transient, explicit and compressible, and the full fan, obstruction and test bench geometries are included in the simulation domain. The fan is truly rotating during the simulations using a Local Reference Frame (LRF) approach [8]. The transient turbulent flow field and its radiating flow-induced noise contributions are simultaneously predicted and no coupling with an acoustics propagation solver is required [9]. The acoustic power corresponding to the BPF contribution is calculated by performing a spectral signal processing of the pressure time histories at microphones location. Based on the simulations results and a Kriging Response Surface Model, an Adaptive Sampling approach derived from the Weighted Expected Improvement Function (WEIF) [10] is used iteratively to investigate unexplored areas of the design space, to target high potential areas in the response surface and to converge as fast as possible towards the most efficient flow obstruction designs.

Considering the high performances of the CFD/CAA solver, the complete design process involving full 3-D transient and accurate aeroacoustics simulations are performed over a few days period. This is a critical aspect in the sense that this optimization method satisfies the fast turnaround times associated with the development cycles and can then be considered as a real alternate design solution.

The design parameters, the CFD/CAA approach and some insight on the optimization method are provided in the first section. The second section focuses on the results of the design process. The analysis of the underlying flow physics and noise reduction phenomena is discussed in the last section of the paper.

NUMERICAL APPROACH

Lattice Boltzmann Method

The CFD/CAA solver PowerFLOW is used to compute compressible and unsteady flow physics. The code is based on the Lattice Boltzmann Method (LBM). Lattice based methods were proposed a couple of decades ago [2-4] as an alternative numerical method to traditional Computational Fluid Dynamics (CFD). Unlike conventional methods based on discretizing the macroscopic continuum equations, LBM relies on the Boltzmann kinetic equation at the "mesoscopic" scale in order to predict macroscopic fluid dynamics. The Very Large Eddy Simulation (VLES) coupled with a modified k-ε two-equation model is incorporated in the LBM approach. Near wall flow is treated with an advanced turbulent wall-model that takes into account for pressure gradients. This model is based on the generalized law of wall which is iteratively solved to provide an estimation of the wall-shear stress.

For simulations of flow with arbitrary geometry rotating in time around a fixed axis, the 3-dimensional computational domain can be divided into an inner and an outer domain. The inner domain has a grid fixed with the rotating geometry so that the geometry does not have a relative motion with respect to the grid. This forms a "body-fixed" Local Reference Frame (LRF) domain with the rotating geometry. The grid in the outer domain is fixed with the ground and forms a "ground-fixed" reference frame domain. Between the inner domain and outer domain, there is a closed transparent interface to connect fluid flows. The implementation of this interface region is presented in [8]. Examples of application can be found in [11-13].

Numerical setup

This study relies on the six blades backward centrifugal fan discussed in [1]. The entire system is simulated including the bench, the fan and the flow obstruction, as illustrated in Figure 1. The heat exchanger is modeled as a porous medium which pressure loss is defined as a function of the mass flow and derived from the performance curve of the real exchanger. The grid resolution used is the same as in [1] and can be found in the referenced paper.

Fan rotation is imposed and set to 2200 RPM. Pressure boundary conditions are applied to the boundary of the simulation domain and atmospheric pressure is imposed. The simulation domain includes sponge zones to avoid any spurious reflections of acoustic wave from the boundary conditions. The total physical time simulated is T_{tot} = 0.682 s, which corresponds to approximately 25 fan rotations. For the finest grid resolution, the time step is Δt = 3.3x10^{-6} s. The Reynolds number based on the blade chord length and the tip velocity is Re_c = 1.94x10^{6}, and the Mach number based on the tip velocity is M_t = 0.194.

Pressure histories are recorded during the simulation at the four microphones locations represented in Figure 1 and the maximum frequency that can be captured at this location is ~10 kHz [1].

Acoustic Power radiated by the system is derived from Power Spectral Density with a Δf = 10 Hz bandwidth computed at microphones locations. The Blade Passing Frequency (BPF) level is extracted and is used as the objective function for the optimization process. The average mass flow rate passing through the fan is evaluated for monitoring purposes.

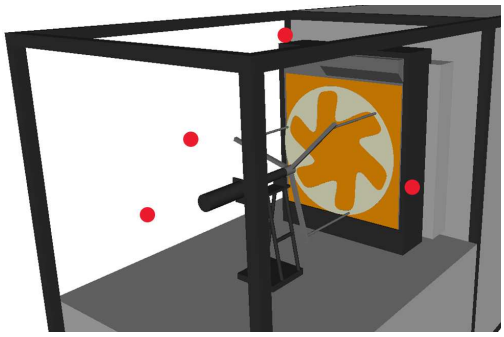

Figure 1: Microphones location used to evaluate the acoustic power of the BPF noise.

Optimization method

Since reducing product development cycles is one of the major constraints for manufacturers in the fan industry, an iterative approach is used in this study. Unlike conventional Design of Experiments (DoE), intermediate results of the ongoing study are used to refine the model representing the response of the system. This allows a faster convergence to efficient configurations and reduces the number of simulations. The process can be described in three steps:

The first step of this process is the Initial Characterization. The aim of this first step is to explore the design space and guide upcoming iterations. N + 2 sets of parameters are generated using a Uniform Latin Hypercube distribution, which guarantees to be relatively uniform over each dimension. Based on the results of these simulations, a response surface is built using a Kriging surface model.

The second step consists in investigating unexplored areas of the design space and targeting high potential areas in the response surface using an Adaptive Sampling (AS) approach. Derived from the Weighted Expected Improvement Function (WEIF) described by Sobester et al. [10]. More details on this process can be found in Sun et al. [14]. The concept of this method is to generate new configurations, simulate them and integrate the results in the data set. From there, the response surface is updated and the same process is repeated, leading to an iterative refinement of the response surface.

As a third step, a local refinement of the response surface can be performed at any time by manually choosing and simulating any configuration predicted by the response surface model. This capability can be used to validate the global optimum predicted by the response surface model or to find the best compromise between two objective functions.

Design parameters

Designing and calibrating a flow obstruction for a new fan or a complete system represents a real challenge for manufacturers as it requires time and human effort to manually adjust the device parameters. In this study, four geometry design features and one calibration parameter are used to automatically design optimized flow obstructions from a generic geometry.

Starting from an outer 20 mm wide ring with the same diameter as the fan, the geometry tool PowerDELTA 2.2 is used to apply four types of deformation by morphing the mesh of the ring. A 6-lobes axisymmetric pattern is generated by adjusting the lobes height, the width of both sides of the lobes and introducing a forward or backward orientation of the lobes. Scaling factors are used to control the amplitude of the deformation for each morphing feature and are set as inputs for the optimization process. The angular orientation of the flow obstruction playing a significant role on the BPF levels [1] varies in the range [0, 60] degrees and corresponds to the fifth input of the optimization process. The axial distance to the heat exchanger is set to 20 mm similarly to [1]. In Figure 2, the original outer ring and the minimum and maximum deformations applied to the obstruction geometry is shown, giving an idea of the design space that can be explored.

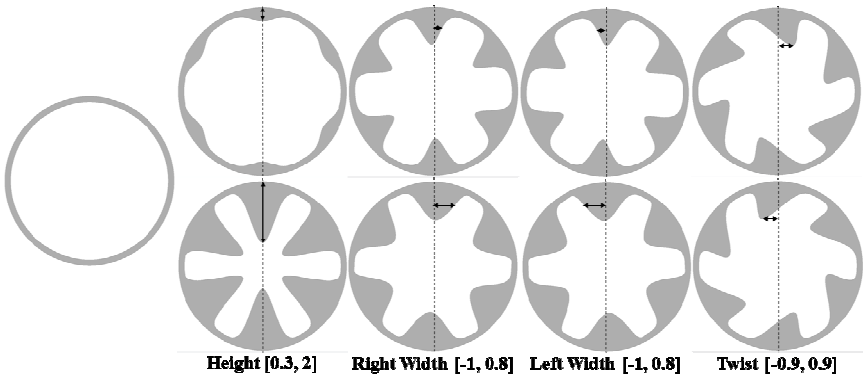

Figure 2: Left: Generic ring geometry. Top: Minimum deformation. Bottom: Maximum deformation.

OPTIMIZATION RESULTS

Considering that the manually optimized flow obstruction studied in [1] already provides the best achievable acoustic power BPF level (75.6 dB) and an acceptable airflow penalty (2.5%), the objectives of this optimization is to design and calibrate flow obstructions achieving an acoustic power BPF level of 76-78 dB and an airflow penalty in the 2-4% range in a realistic product development time frame.

Initial Characterization and Adaptive Sampling iterations

As described in the previous section, the first step of the optimization process is the Initial Characterization. Considering five optimization parameters, seven sets of parameters are generated using a Uniform Latin Hypercube distribution. After simulating these configurations, the second step consists in five Adaptive Sampling iterations (AS), including the simulation of three new configurations per iteration. A total of 22 configurations are simulated. Figure 3 presents the distribution of the parameters sets in the design space for all iterations and shows that a large portion of the design space is explored.

The evolution of the parameters values through the AS iterations can be used to derive parameter trends. For instance Figure 3 shows that the last two iterations (6 configurations) are designed using positive and relatively high Twist values. For these cases, the obstruction lobes are following the fan rotation and positively impact the system response. No particular trend is observed on the angular position distribution. This is expected since the optimal angular position is different for each obstruction design.

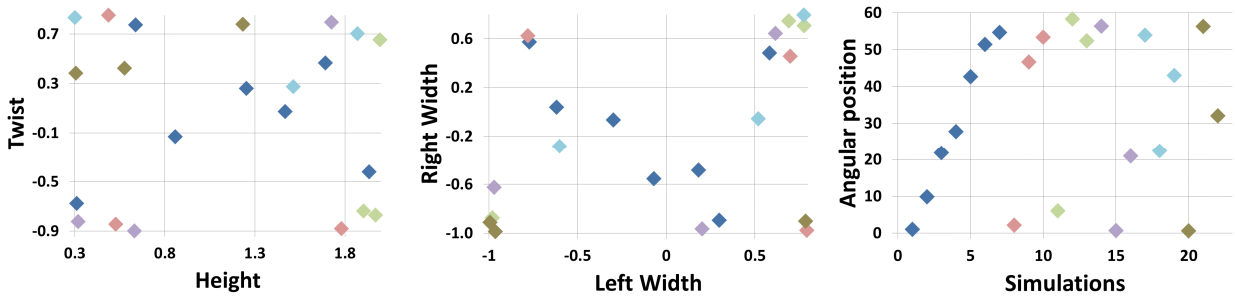

Figure 3: Parameters distribution in the Design Space for the first 22 configurations. Left: Height and Twist. Middle: Left Width and Right Width. Right: Angular position

◆: Initial Characterization. ◆: AS 1. ◆: AS 2. ◆: AS 3. ◆: AS 4. ◆: AS 5.

The aeroacoustics and airflow performance of the 22 configurations are presented in Figure 4. The simulated acoustic power BPF levels are within a 10 dB range, highlighting the effects of the flow obstructions on the radiated tonal contribution. Two promising designs emerge from this study

corresponding to Configuration 19 (77.2 dB, -1% airflow) and 22 (77.5 dB, +2% airflow). For these two, the acoustic performances are in the initial 76-78 dB objective range and the corresponding airflow are also in a very satisfying range, particularly for Configuration 22 due to its opened shape.

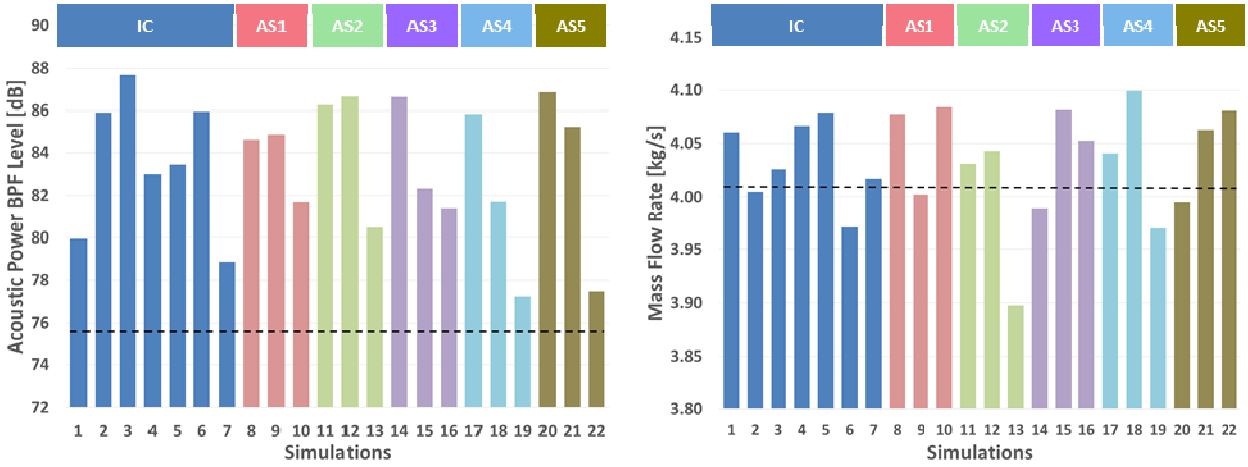

Figure 4: Left: Acoustic Power BPF level in dB ($dB_{ref} = 10^{-12}$ W). Right: Mass Flow Rate in kg/s. The results for the manually optimized obstruction [1] are represented with a dashed line

The acoustic power spectrum around the BPF for the Configuration 19 and 22 are plotted in Figure 5, and compared to the reference configuration. The configurations 19 and 22 present slightly higher levels at the blade passing frequency but their overall acoustic performance is very similar to the manually optimized configuration.

Considering that less than a business week was required to obtain these results, it makes this automated digital process an interesting alternative to design optimized flow obstructions.

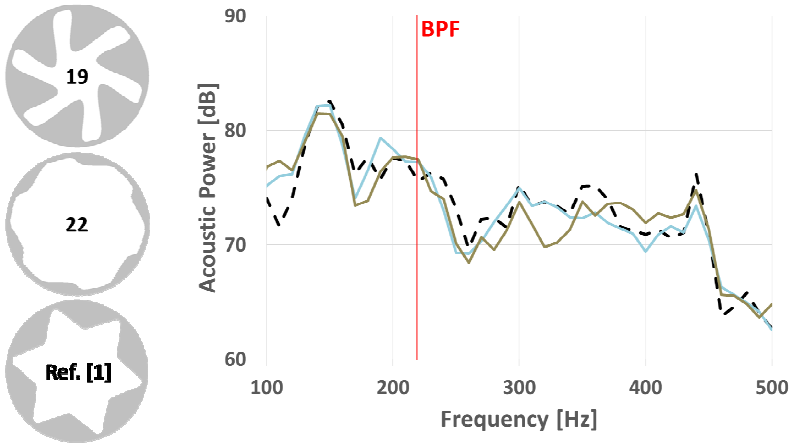

Figure 5: Top Left: Simulation 19. Middle Left: Simulation 22. Bottom Left: Reference [1] Right: Acoustic Power spectrum. Simulation 19. Simulation 22. Manually optimized [1].

Response Surface exploration

Although the previous automated process provides satisfying designs in a short development cycle, exploring manually the response surface can help to further improve the system performance. To provide a representation of the Kriging based response surface model, a fine sampling is performed. 20 000 configurations are generated using a Uniform Latin Hypercube distribution. Acoustic power BPF levels and mass flow rates are evaluated for each of the 20 000 configurations and the corresponding results are plotted with black dots in in Figure 6. The 22 simulated configurations are

represented with red dots and the manually optimized configuration from [1] is represented with a green dot.

It is shown that very few configurations on the response surface have better acoustic performance than the manually optimized design. This is expected since this design provides the best achievable acoustic power BPF level. Some configurations on the top left of the cloud of points can be expected to provide better airflow performances with almost comparable acoustic response. To confirm this possibility three configurations are chosen in the area of interest of the response surface and are represented with orange dots in Figure 6.

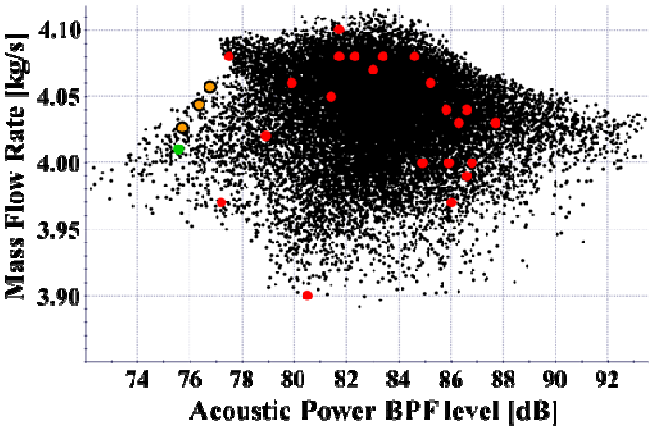

Figure 6: Mass flow rate versus Acoustic power BPF level map.

● *Estimated configurations.* ● *Simulated configurations.* ● *Reference configuration [1].* ○ *Additional configurations.*

The simulation results of the three additional configurations are reported in Table 1 and compared to previously estimated performances. Overall a good agreement within 0.5% is obtained in the comparison of estimated and simulated mass flow rates. The simulated acoustic power BPF level of Configuration 23 and 24 are in satisfying agreement with the estimated results, within 1.6 dB. Considering that the Configuration 25 has a higher BPF level than estimated, this highlights the sensitivity of the system and that more simulations would be required to further improve the response surface.

Table 1: Comparison of estimated and simulated results for the manually selected configurations

Configuration	Estimated Acoustic Power BPF level [dB]	Simulated Acoustic Power BPF level [dB]	Estimated Mass flow rate [kg/s]	Simulated Mass flow rate [kg/s]
23	76.7	78.3	4.06	4.04
24	76.3	76.5	4.04	4.04
25	75.8	80.8	4.02	4.01

The best configuration obtained using this process is Configuration 24. Compared to the manually optimized configuration (75.6 dB, 4.01 kg/s), a slightly higher mass flow rate is obtained and the acoustic power BPF level is less than 1 dB from the best achievable level. This confirms that in addition to a fully automated process, further improvements can be achieved by taking advantage of the response surfaces and manually choosing configurations in interesting areas.

NOISE REDUCTION ANALYSIS

This section aims at analyzing the underlying flow physics at the origin of the tonal noise reduction brought by the flow obstructions. To focus on the most salient effects, the analysis of the mechanisms is focused on the worst and best acoustically performing obstructions, Configuration 3 and 24 respectively (see Figure 7).

Radiated tonal noise

Figure 7 presents the acoustic power spectra for Configurations 3 and 24. The BPF noise level is reduced from 87.7 dB (Configuration 03) to 76.5 dB (Configuration 24). This configuration is therefore very promising since it shows almost no contribution from the blade passing frequency. The effect on broadband noise and subharmonics is very limited, as observed in [1].

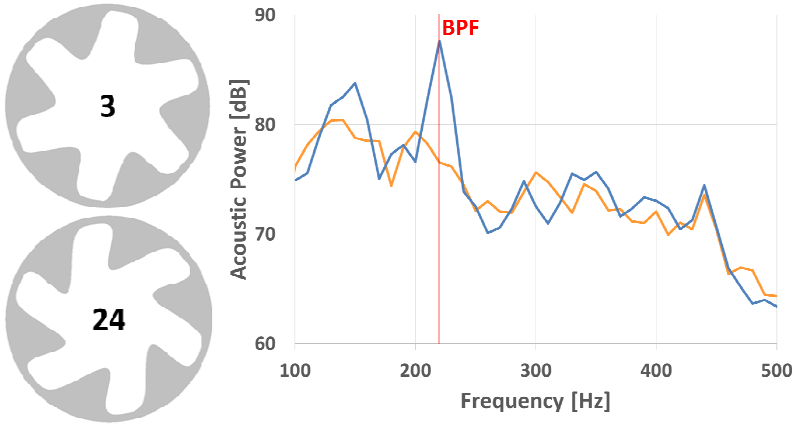

Figure 7: Acoustic Power spectrum. —Configuration 3. —Configuration 24. —Blade Passing Frequency.

Figure 8 presents the intensity of pressure fluctuations in decibels on vertical and horizontal planes, so called dB maps, centered on the fan axis and filtered around the fan BPF. The vertical plane shows that the BPF contribution is radiated mainly towards the ground and diffraction effects are visible. The radiated noise at the BPF in the horizontal plane do not present any privileged direction and looks almost monopolar. The optimized flow obstruction in Configuration 24 reduces the fan radiated BPF contribution in all directions and no particular effect on directivity is observed.

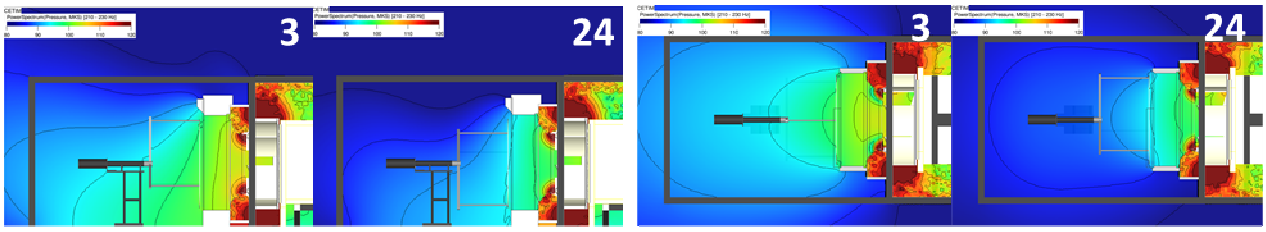

Figure 8: dB Map on a vertical and horizontal planes centered on the fan axis and filtered around the BPF.

Ingested Flow Topology

In the case of rotating fans, radiated tonal noise is closely related to the ingestion of a non-uniform flow, often due to installation effects. [2, 15]. Since the obstruction has a significant impact on the BPF contribution, transient and spectral analysis are performed to better characterize the fan incoming flow and its effect on the fan blades.

As the fan in this study is in installed condition, the incoming flow is strongly non uniform. In both configurations, the proximity of the heat exchanger frame is creating pairs of steady flow structures on the sides and at the top of the shroud convergent, as highlighted by instantaneous isosurfaces of

Lambda2 criterion for Configuration 3 in Figure 9. Time animations reveal that these structures are sliced by the fan blades creating flow perturbations on both pressure and suction sides of the blades.

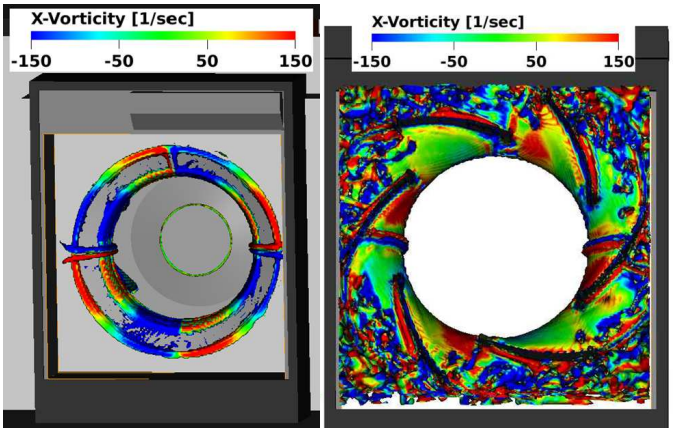

Figure 9: Configuration 3: Instantaneous isosurface of Lambda 2 criterion colored by X-Vorticity (flow direction).

Instantaneous isosurfaces of X-Vorticity (flow direction) are presented in Figure 10. For both configurations, the flow obstructions lobes are creating 6 pairs of steady vorticity tubes which are also ingested by the fan. The relative position of the vorticity tubes to the flow structures coming from the heat exchanger frame is however different. In Configuration 3, the vorticity tubes coming from the sides end up almost exactly at the same position as the structures coming from the heat exchanger frame, creating a bigger flow perturbation interacting with the blades. In Configuration 24, the side vorticity tubes end up right after the heat exchanger frame structures so that the fan blades slice these structures in a first time and interact with the tubes in a second time.

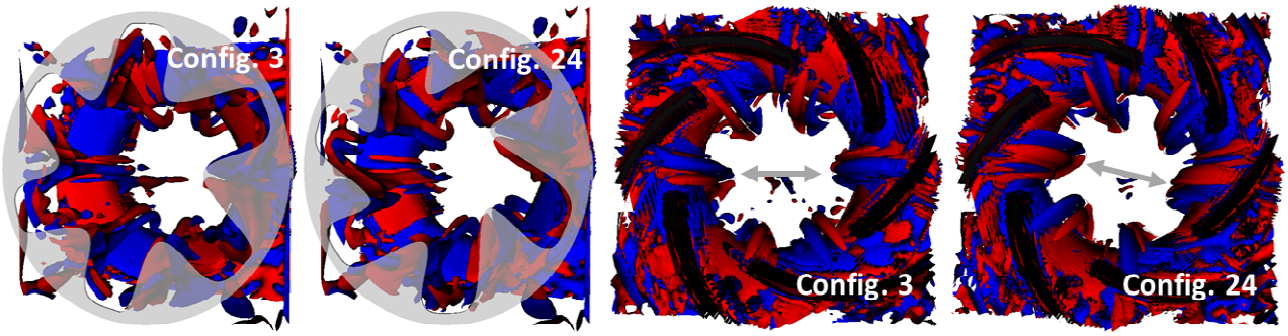

Figure 10: Instantaneous isosurface of X-Vorticity (flow direction). Blue: $\omega_- = -60\ s^{-1}$. Red: $\omega_+ = 60\ s^{-1}$.

This analysis confirms that not only the fan sees a non-uniform incoming flow due to installations effect but the flow obstructions introduce additional perturbations interacting with the fan blades. Since acoustic analogy methods, based for instance on the Ffowcs-Williams and Hawkings equation, rely on the unsteady pressure field on surfaces to predict radiated noise in the far field, characterizing the effects of the flow perturbations on the blades unsteady pressure field can give indication of their potential effects on the radiated BPF contribution.

Instantaneous isosurfaces of X-Vorticity as well as pressure fluctuations filtered around the fan BPF on the blade surface are plotted in Figure 11 at four different time frames representing a blade passage, and focusing on the structures coming from the sides of the convergent. At time T1, before reaching the side perturbation, both configurations show some pressure fluctuations on the leading edge on the blades, probably coming from the interaction with the previous vorticity tube. At time T2, just before reaching the perturbation, Configuration 3 shows almost no pressure fluctuations whereas some are still visible on Configuration 24, probably because of its interaction with the previous perturbation. When reaching the side perturbation at T3, a strong pressure fluctuation is

observed on Configuration 3 but the one on Configuration 24 is of much lower magnitude. Finally both configurations show low fluctuations levels after the blade passage at T4.

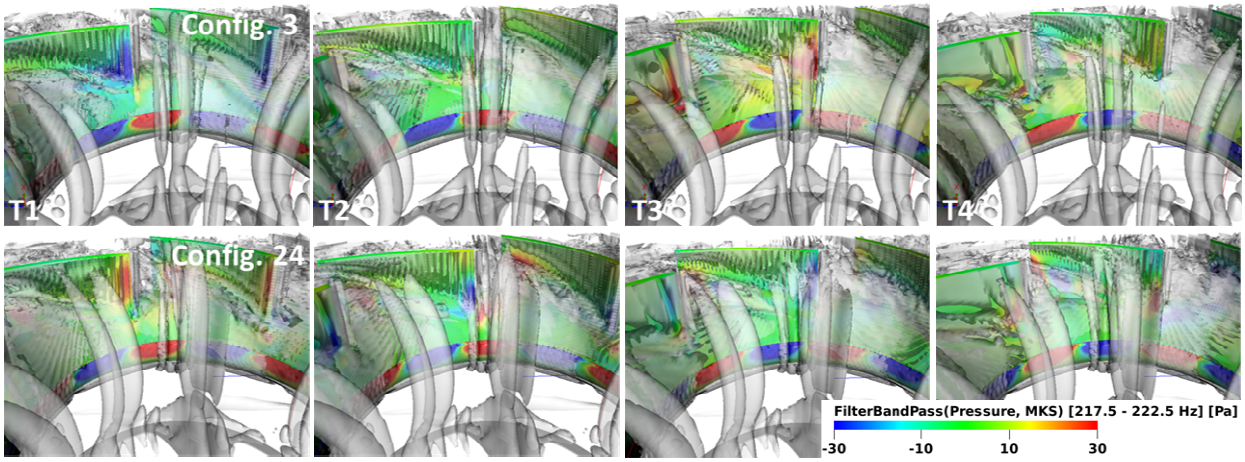

Figure 11: Transparent white: Instantaneous isosurfaces of X-Vorticity (flow direction). Colored: Surface pressure fluctuations on the blades filtered around the fan BPF.

In the case of Configuration 3, the vorticity tube coming from the flow obstruction covers the flow structure coming from the heat exchanger frame, creating a precisely located perturbation. This seems to intensify the resulting pressure fluctuations. In the case of Configuration 24, not only the blade reaches the flow perturbation with remaining pressure fluctuations from the previous vorticity tube but the perturbation itself is larger and less coherent. This lack of coherence seems to positively impact the pressure fluctuations observed at the blade surface and reduce the effect of the flow structure coming from the heat exchanger frame.

Fluctuating Lift field

Radiated tonal noise is related to the unsteady lift distribution on the blades generated by the ingestion of a non-uniform flow by the fan [2, 3]. Further analysis not presented in this paper confirm that the effects of the incoming flow on the blades pressure fluctuations filtered at the BPF (Figure 11) are also observed on the blades fluctuating lift filtered at the BPF.

In order to evaluate the overall intensity of the lift fluctuations on the fan blades, transient lift signals are integrated over each blades resulting in a single lift signal for each blade. A Fast Fourier Tranform (FFT) is performed to evaluate the intensity of the integrated lift fluctuations in the spectral domain for each blade. Figure 12 presents the lift spectrum averaged over the 6 blades for Configuration 3 and 24. The two configurations show very similar lift fluctuations except at the BPF where a significantly lower level is observed for the best configuration. In this case, and as shown in the acoustic power spectrum the BPF, the tonal contribution is almost not discernable from the other contributions. This confirms that the overall lift (or pressure) fluctuations on the blades are significantly lower at the BPF for the best configuration.

This analysis highlights the effects of the flow perturbations generated by the flow obstructions and ingested by the fan. Their interactions with the flow structures coming from the heat exchanger frame seems to have a significant influence on the resulting force and pressure fluctuations on the blades at the BPF. But their overall effect on the acoustic power BPF level might imply other interactions between the incoming flow and the blades. Further analysis is required to fully understand the differences in the unsteady flow around the blades and the noise reduction mechanisms.

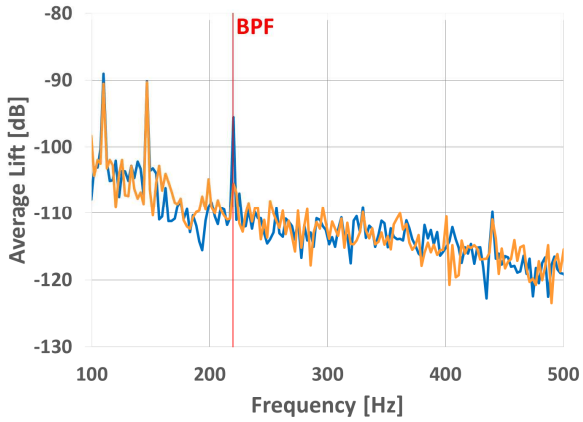

Figure 12: Averaged lift power spectrum. *Configuration 3.* *Configuration 24.* *Blade Passing Frequency.*

CONCLUSIONS

An efficient and automated digital process for designing and calibrating optimized flow obstructions in a short development time frame is presented. Such passive noise control devices are known to significantly reduce the Blade Passing Frequency noise caused by the ingestion of a non-uniform flow by a fan in installed conditions. Designing and calibrating this device for new fan designs or completely new systems traditionally requires extensive and time consuming tests campaigns relying on a tries-and-errors approach and numerous prototypes, representing for manufacturers significant constraints during development.

In the present study, four geometry features based on morphing are used to generate flow obstruction designs from a generic outer ring geometry. The angular orientation of the flow obstructions is used for their calibration, forming a 5 dimensions design space. The passive noise control devices are placed upstream a production fan-heat exchanger system in installed conditions. The resulting 3-D turbulent flow and the induced acoustic response are respectively simulated and evaluated using the transient and compressible CFD/CAA solver PowerFLOW.

After a first exploration of the design space by simulating seven uniformly distributed configurations, a Kriging model is used to derive the response surface characterizing the effect of the five parameters of the study on the acoustic power BPF noise level. Based on these results, an iterative Adaptive Sampling approach is used to investigate unexplored areas of the design space, to target high potential areas in the response surface and to converge as fast as possible towards the most efficient flow obstruction designs. Five iterations including three configurations each are simulated, resulting in a total of 22 simulations. The best flow obstruction designed and calibrated using this automated digital process presents an acoustic power BPF level within 2dB compared to a manually optimized configuration and slightly better airflow performances. Requiring less than a business week to complete, this automated digital process is able to provide calibrated flow obstructions almost as efficient as manually optimized designs.

In order to leverage the response surface model and to try to further improve the system performances, three additional configurations are manually chosen by looking at the acoustic and airflow responses. Whereas the airflow performances predictions of the response surface are confirmed by 3-D simulations, the acoustic response showed more sensitivity, highlighting the need for more configurations to improve the accuracy of the acoustic response surface. However, the best acoustic and airflow performances are obtained for one of these configurations. Although the automated digital process already provides efficient solutions in a product development time frame, further improvement can be achieved by manually exploring the response surface.

Transient simulations results of the configurations showing the best and worst acoustic performances are analyzed to give some insight on the noise reduction mechanisms provided by the flow obstructions. The two flow obstructions are shown to introduce vorticity tubes in the flow ingested by the fan and interact differently with flow structures coming from the heat exchanger frame. On the worst configuration, vorticity tubes seems to intensify the coherence of the flow perturbation, resulting in higher pressure fluctuation levels on the fan blades. On the best configuration, the fan blades seem to face a larger and less coherent flow perturbation, resulting is much lower pressure fluctuation levels. However the overall impact of the flow obstructions on the radiated acoustic power BPF level may imply other flow interactions and further analysis would be require to fully understand the noise reduction mechanisms.

BIBLIOGRAPHY

[1] F. Pérot, M.-S. Kim, V. Le Goff, X. Carniel, Y. Goth, C. Chassaignon – *Numerical optimization of the tonal noise of a backward centrifugal fan using a flow obstruction*, Noise Control Engr. J., 61, 3, May-June, **2013**.

[2] A. Gérard, A. Berry, P. Masson, Y. Gervais – *Experimental validation of tonal noise control from subsonic axial fans using flow control obstructions*, Journal of Sound and Vibration, Vol. 231, no. 1-2, pp. 8-25, **2009**.

[3] A. Gérard, A. Berry, P. Masson, Y. Gervais – *Modelling of tonal noise control from subsonic axial fans using flow control obstruction*, Journal of Sound and Vibration, Vol. 231, no. 1-2, pp. 26-44, **2009**.

[4] A. Gérard, A. Berry, P. Masson, S. Moreau – *Use of a beat effect for the automatic positioning of flow obstructions to control tonal fan noise: Theory and experiments*, Journal of Sound and Vibration, Vol. 332, no. 19, pp. 4450-4460, **2013**.

[5] S. Chen, G. Doolen – *Lattice Boltzmann method for fluid flows*, Ann. Rev. Fluid Mech., vol. 30, pp. 329-364, **1998**.

[6] H. Chen – *Volumetric Formulation of the Lattice Boltzmann Method for Fluid Dynamics: Basic Concept*, Phys. Rev. E, Vol. 58, pp. 3955-3963, **1998**.

[7] H. Chen, S. Orzag, I. Staroselsky, S. Succi – *Expanded analogy between Boltzmann Kinetic Theory of Fluid and Turbulence*, J. Fluid Mech., Vol 519, pp 301-314, **2004**.

[8] R. Zang, Y. Li, C. Sun, R. Satti, R. Shock, J. Hoch, H. Chen – *Lattice Boltzmann approach for Local Reference Frames*, Communications in Computational Physics, 9, pp. 1193-1205, **2011**.

[9] G. A. Brès, F. Pérot, D. Freed – *Properties of the Lattice-Boltzmann Method for Acoustics*, 15th AIAA/CEAS Aeroacoustics Conference, Miami, FL, **2009**.

[10] A. Sobester, S. J. Leary, A. J. Keane – *On the design and optimization strategies based on global response surface approximation models*, Journal of Global Optimization, 33, pp. 31-59, **2005**.

[11] F. Pérot, M.S. Kim, K. Wada, K. Norisada, M. Kitada, S. Hirayama, M. Sakai, S. Imahigasi, N. Sasaki – *HVAC blower aeroacoustics predictions based on the Lattice-Boltzmann Method*, AJK Conference, AJK2011-23018, Hamamatsu, Japan, **2011**.

[12] F. Pérot, M.S. Kim, S. Moreau, D. Neal – *Investigation of the Flow Generated by an Axial 3-Blade Fan*, 13th ISROMAC Conference, 2010-082, Honolulu, Hawaii, **2010**.

[13] F. Pérot, M.S. Kim, S. Moreau, M. Henner, D. Neal – *Direct Aeroacoustics Prediction of a Low Speed Axial Fan*, 16th AIAA/CEAS Aeroacoustics Conference, AIAA-2010-3887, Stockholm, Sweden, **2010**.

[14] S. Sun, Y.-P. Chang, Q. Fu, J. Zhao, L. Ma, S. Fan, B. Li, A. Shestopalov, P. Stewart, H. Friz – *Aerodynamic shape optimization of an SUV in early development stage using a response surface method*, SAE Intl. J. Passeng. Cars-Mech. Syst., 7(4), pp. 1252-1263, **2014**.

[15] M. Sturm, M. Sanjosé, S. Moreau, T. Carolus – *Aeroacoustic simulation of an axial fan including the full test rig by using the Lattice Boltzmann Method*, Fan2015 Conference, Lyon, France, **2015**.